



## Sol-gel, Hydrothermal, and Combustion Synthetic Methods of Zinc Oxide Nanoparticles and Their Modification with Polyaniline for Antimicrobial Nanocomposites Application



S.M.M. Morsi<sup>1</sup>, R.M. Mohsen<sup>1\*</sup>, M.M.Selim<sup>2</sup>, H.S. El-Sherif<sup>1</sup>

<sup>1</sup>National Research Centre, Polymer and Pigments Department, 33 El Bohoth St. (Former El Tahrir St.), Dokki, P.O. 12622, Giza, Egypt.

<sup>2</sup>National Research Centre, Physical Chemistry Department, 33 El Bohoth St. (Former El Tahrir St.), Dokki, P.O. 12622, Giza, Egypt.

ZINC oxide nanoparticles (ZnO NPs) have attracted much medical attention as antibacterial agents through their ability to produce reactive oxygen species (ROS) under ultraviolet light. Conducting polymers can enhance the photocatalytic efficiency of ZnO NPs by expanding their absorption in the visible region. In this article, ZnO NPs were prepared and characterized using three different chemical routes; sol-gel, hydrothermal, and combustion methods. The effect of calcination temperature on their properties had been investigated. ZnO NPs prepared from the combustion method at 750 °C was modified with (10%, 15%, and 20%) polyaniline (PANI) by *in-situ* polymerization of aniline on the dispersion of ZnO NPs to produce PANI/ZnO nanocomposites (NCs) NC10, NC15, and NC20, respectively. Characterization of the synthesized NCs was carried out by FTIR, XRD, TEM, and SEM. Their antibacterial efficiency toward *Escherichia coli* G- and *Staphylococcus aureus* G+ and antifungal activity to *Aspergillus flavus* and *Candida albicans* were evaluated. The NCs revealed medium antibacterial activity where NC15 showed the highest activity to *Staphylococcus aureus* (G<sup>+</sup>) and *Candida albicans*, however, no efficiency was detected against *Aspergillus flavus* (Fungus).

**Keywords:** Polyaniline, Nanocomposite, Sol-gel, Hydrothermal, Combustion, Antimicrobial activity.

### Introduction

ZnO particles are semiconductor compounds of group II-VI that crystallizes in a wurtzite structure. Their crystal's internal links are a mix of ionic and covalent bonds and therefore, they lay in the boundary between ionic and covalent semiconductors. ZnO is characterized by important properties that made it suitable for use in many advanced applications such as electronics, optoelectronics and laser technology [1,2]. These characteristics include; bond energy of approximately 60 meV, an energy band gap close to 3.37 eV, high thermal and mechanical stability at room temperature, and good piezoelectric and pyroelectric properties. The latter properties allow ZnO to be used as an energy generator,

photocatalyst, sensor, and converter. In addition to all these uses, ZnO is widely used as an antimicrobial agent especially for its low toxicity, biocompatibility, and biodegradability [2-4]. This superior antimicrobial activity generated from its photocatalytic efficiency in producing active species like H<sub>2</sub>O<sub>2</sub> that can penetrate the cell wall of the organism and kill or inhibit the microbe [5]. In this regard, the size of ZnO particles has a significant impact on their final properties. ZnO nanoparticles (NPs) show completely different properties and efficiencies than those in the micron range due to increased surface area and activation of energy [1]. Thus, ZnO NPs have higher ability to penetrate the cell membrane increased efficiency to inhibit the microbe by their

\*Corresponding author e-mail: rajiamohsen@yahoo.com

Received 31/12/2018., Accepted 12/2/2019

DOI: 10.21608/ejchem.2019.6952.1578

©2019 National Information and Documentation Center (NIDOC)

higher interfacial areas and activation energy. Therefore, the preparation of wurtzite hexagonal structure of ZnO in the nanoscale is considered a major challenge for scientists. This includes the selection of reactants, their concentrations, and the reaction condition. For example; the calcination temperature has a great influence on the morphology and the size of the synthesized ZnO [6-9]. Matei et al. [3] presented the most common techniques used for the synthesis of ZnO NPs such as; mechanochemical [10], precipitation [11-13], emulsion [14], sol-gel [15,16], microwave [17], hydrothermal [18], combustion [5,19], sonochemical synthesis [20].

The photocatalytic and photoelectrochemical activity of ZnO NPs can be enhanced by their incorporation with polyaniline (PANI). This enhancement is attributed to the ability of PANI to photosensitize under the visible light energy and thus expands the wavenumber absorption region of ZnO NPs. In addition, PANI forms a bridge-like structure and type-II heterojunction (staggered gap) with ZnO NPs. This leads to an efficient separation and faster transfer of photoinduced charge carriers at the interface [21].

Many papers studied the antimicrobial efficiency of ZnO NPs such as; Kumra et al. [4] studied the antibacterial activity of flower-shaped ZnO NPs towards gram-positive and gram-negative bacteria. Espitia et al [22] reviewed the synthetic methods of ZnO NPs and mechanisms of their antimicrobial action. Few researchers studied the antibacterial activity of PANI/ZnO nanocomposites (NCs) such as; Kermani et al [23] studied the antibacterial activity of ZnO NPs and polyvinylalcohol/PANI/ZnO NC. Khan et al. [24] proved the high antibacterial activity PANI/ZnO nanocomposite against gram-negative and gram-positive bacteria. Hou et al. [25] carried out the antibacterial activities of Ag-doped ZnO/PANI NCs. Hence, to the best of our knowledge, there is a lack of the PANI/ZnO NCs antifungal activity.

In this research article, the antifungal beside the antibacterial activity of PANI/ZnO NCs was studied. Firstly, ZnO NPs were synthesized using different chemical methods; sol-gel, hydrothermal, and combustion methods to select the most major wurtzite hexagonal structure sample. General investigation on the effect of calcination temperature on the characterization properties was carried out. PANI/ZnO NCs were synthesized by *in-situ* polymerization of aniline on the dispersion of ZnO NPs followed

by characterization of their properties. Their antimicrobial activity of the NCs was evaluated to optimize the suitable PANI concentration in the NCs that gives the highest efficiency.

## **Experimental**

### *Materials*

Zinc acetate dihydrate 99.5% and Zinc nitrate hexahydrate 99% were obtained from SISCO Research Laboratories Pvt. Ltd. and Merck, respectively. Urea was supplied from El Delta Co. for Fertilizers & Chemical Industries, Talkha, Egypt. Ethyl alcohol 99% was purchased from Sigma-Aldrich. Sodium hydroxide pellets 99% was provided from Laboratory Chemicals, Modern Lab. Aniline monomer purchased from Sigma-Aldrich Company was distilled in rotary evaporator under reduced pressure before use. Potassium persulfate 98%, ethylene glycol, and hydrochloric acid 35-38% were purchased from Fischer Laboratory Reagent, SDFCL Fine Chemical Ltd. Cambrian Chemicals, respectively.

### *Methodology*

#### *Preparation of ZnO NPs*

Three methods were used to synthesize ZnO NPs [3]; sol gel, hydrothermal and combustion methods mentioned as (M1), (M2) and (M3), respectively.

#### *a. Sol-gel method (M1)*

It is the simplest method and has the advantage of controlling the morphology and particle size through the reaction parameters. Synthesis is carried out by hydrolysis of zinc acetate dihydrate as a precursor in presence of ethanol as solvent. In this method 5g zinc acetate dihydrate is dissolved in 100 ml doubled distilled water with continuous stirring. The temperature of the solution was raised to 50°C at which 300 ml absolute ethanol was slowly added with continuous stirring. The temperature of the reaction was raised to 80°C and kept under reflux for 5 hours. The solution was evaporated and the obtained white precipitate was washed, filtered and dried at room temperature. The product was calcinated at 300°C and 500°C for two hours in a heating muffle and will be referred as ZnO-M1 (300°C) and ZnO-M1 (500°C).

#### *b. Hydrothermal method (M2)*

In this method, 10g zinc acetate dihydrate was dissolved in 200 ml double distilled water and 500 ml of absolute ethyl alcohol with continuous stirring. The hydrolysis reaction was obtained by

adding NaOH solution was added to adjust the pH at 9. The reaction solution was refluxed at 80°C. A white precipitate was obtained, filtered and washed, dried at room temperature. The calcination process of the product was carried out, without calcination and at 500 °C for 2 hours in a muffle furnace, and will be referred as ZnO-M2 (without calcination) and ZnO-M2 (500°C), respectively.

*c. Combustion method (M3) or selfpropagation high temperature*

This method is an effective low cost technique for useful substances production. It is a popular method to prepare materials both in the nanoscale and at a high yield. The reaction was carried out by mixing zinc nitrate hexahydrate as an oxidant with urea as a fuel at a molar ratio of 4:1. The powder mixture was dissolved in a little amount of double distilled water until a paste was formed. The latter was gently heated on a hot plate forming a thick viscous gel. The gel was further heated in a furnace muffle at 750°C and 900°C for two hours to remove the carbonaceous materials. The two ZnO NPs product will be referred as ZnO-M3 (750°C) and ZnO-M3 (900°C).

*Synthesis of HCl-doped PANI*

HCl-doped PANI was synthesized by *in-situ* chemical oxidative polymerization of aniline using HCl and potassium persulfate as a dopant and an oxidizing agent, respectively [5,26]. The molar ratio of aniline to HCl to potassium persulfate is 1: 2.5: 0.3. 3.72 g aniline was added to a round bottom flask filled with 100 ml distilled water and acidified with 8.6 ml HCl. The flask was stirred magnetically for 15 min. 3.24 g potassium persulfate dissolved in 75 ml distilled water was poured into the flask. The reaction was carried out in an ice bath at nearly 4°C for 12 h with a magnetic stirrer. A dark greenish precipitate was obtained, filtered, washed with distilled water, and finally dried at 80°C in an oven.

*Synthesis of PANI/ZnO nanocomposites (PANI/ZnO NCs)*

ZnO NPs produced from M3 at calcination temperature 750°C (ZnO-M3 (750°C)) was used to prepare the PANI/ZnO NCs. The NCs were prepared by oxidative polymerization of aniline (as mentioned in 2.2.2.) in a dispersion of ZnO NPs. The aqueous dispersion of ZnO NPs was prepared by stirring ZnO NPs in distilled water using 5% concentration of ethylene glycol as a stabilizer. The amount of ZnO NPs was 10, 15 and 20 weight % of aniline monomer to produce

NC10, NC15, NC20, respectively. The NCs was in the form of dark greenish precipitates which was filtered, washed, and dried at room temperature.

*Instrumental analysis*

*X-ray powder diffraction (XRD)*

XRD patterns were recorded at room temperature using Philips PW 1390 Diffractometer using Ni-filter and CuK radiation source ( $\lambda = 1.54 \text{ \AA}$ ), Japan, and operated at 40 kV and 40 mA in the  $2\theta$  range 5-80° at the scan speed of 0.05° per second. The average crystallite size (D) is estimated from Scherrer's equation [27]. The lattice strain ( $\epsilon$ ), lattice constant (c), Zn–O bond length (L), dislocation density ( $\delta$ ), Young's modulus, and Williamson–Hall analysis were estimated [5,27].

*Transmission electron microscope (TEM)*

TEM images were examined by using JEOL JX 1230 technique with micro-analyzer electron probe, Japan.

*Scanning electron microscope (SEM)*

SEM micrographs were carried out by Quantum Field Emission Gun 250.

*Fourier transform infrared (FTIR)*

FTIR spectra were obtained by JASCO FTIR 6100 in the range of 4000-400  $\text{cm}^{-1}$  using KBr pellets.

*Antimicrobial activity measurements*

Antimicrobial tests toward (*Escherichia coli G* and *Staphylococcus aureus G*<sup>+</sup>) and (*Asprigillus flavus* and *Candida albicans*) were determined using modified Kirby-Bauer disc diffusion by Hioki 3522-50 LCR Hitester (Japan) [28]. Mueller–Hinton agar is used for determination of susceptibility of microorganisms to antimicrobial agents. Measurements were carried out at "Micro Analytical Center," Faculty of Science, Cairo University. Measurements were carried out at "Micro Analytical Center", Faculty of Science – Cairo University.

## **Results and Discussions**

*FTIR of the prepared ZnO NPs*

The FTIR spectra of the ZnO NPs prepared by the sol-gel method at a calcination temperature of 500°C (ZnO-M1 (500°C)), the hydrothermal method at a calcination temperature of 500°C (ZnO-M2 (500°C)), and the combustion method at a calcination temperature of 750°C (ZnO-M3 (750°C)) are shown in **Fig. 1**. The two transverse

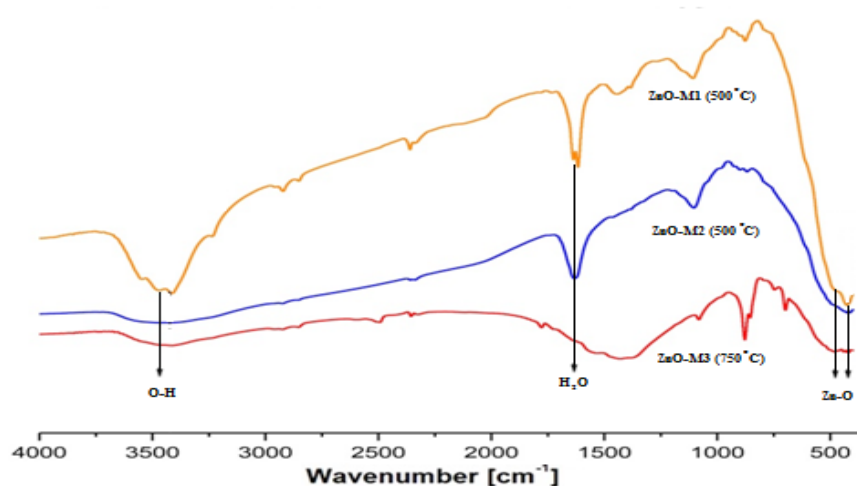


Fig. 1. FTIR of ZnO-M1 (500°C), ZnO-M2 (500°C), and ZnO-M3 (750°C).

optical stretching modes of ZnO is observed at  $\sim 472 \text{ cm}^{-1}$  associated with a strong shoulder at around  $500 \text{ cm}^{-1}$  which confirms the formation of ZnO NPs [29]. Additional absorptions emerged at  $1630 \text{ cm}^{-1}$ ,  $3425 \text{ cm}^{-1}$  and  $1120 \text{ cm}^{-1}$  in the spectra of ZnO-M1, ZnO-M2, and ZnO-M3 due to water, OH on the surface of ZnO NPs and reaction intermediates such as Zn hydroxoacetate complex or zinc acetate cluster ( $\text{Zn}_4\text{O}(\text{CH}_3\text{COO})_6$ ).

#### XRD of the prepared ZnO NPs

XRD patterns of ZnO NPs prepared by the three different methods were illustrated in Fig. 2-4. Generally, the ZnO NPs show the characteristic peaks at  $2\theta = 31.67^\circ$ ,  $34.31^\circ$ ,  $36.14^\circ$ ,  $47.40^\circ$ ,  $56.52^\circ$ ,  $62.73^\circ$ ,  $66.28^\circ$ ,  $67.91^\circ$ ,  $69.03^\circ$ , and  $72.48^\circ$  that are assigned to (100), (002), (101), (102), (110), (103), (200), (112), (201), and (004) planes, respectively. The presence of these peaks indicates that the ZnO NPs were in the polycrystalline wurtzite hexagonal structure (Zincite) (JCPDS 36-1451) [3]. Figure 2 shows the XRD of ZnO-M1 calcinated at  $300^\circ\text{C}$  and  $500^\circ\text{C}$ . The identifying peaks of ZnO NPs are observed in the XRD pattern prepared at  $500^\circ\text{C}$  indicating clear and pure particles. However, the extra peaks formed below  $30^\circ$  in the XRD of ZnO NPs prepared at  $300^\circ\text{C}$  indicate the presence of some impurities in the particles. Figure 3 shows the XRD of ZnO-M2 prepared without calcination and calcinated at  $500^\circ\text{C}$ . The sample prepared without calcination showed a lot of organic impurities due to the precursors used in the synthesis process with the existence of weak peaks indicating the formation of some ZnO NPs. However, the sample prepared at  $500^\circ\text{C}$

exhibited pure ZnO NPs free from any impurities. Figure 4 shows the XRD of ZnO-M3 prepared at calcination temperatures  $750^\circ\text{C}$  and  $900^\circ\text{C}$ . At both temperatures, the formed ZnO NPs are pure and clear without impurities. Therefore, for all the prepared ZnO NPs; ZnO-M1 (calcinated at  $500^\circ\text{C}$ ), ZnO-M2 (calcinated at  $500^\circ\text{C}$ ), ZnO-M3 (calcinated at  $750^\circ\text{C}$ ), and ZnO-M3 (calcinated at  $900^\circ\text{C}$ ) developed the clear and pure XRD patterns. This leads us to conclude that the three methods of preparation can produce highly pure ZnO NPs according to the synthetic conditions.

The crystallite size ( $D$ ) of ZnO NPs was estimated from the width of the most intense peak according to Scherrer's formula. It can be noticed that 101 plane is the strongest diffraction peak which indicates that the ZnO nanocrystals have a preferential crystallographic 101 orientation. The crystallite size of ZnO-M1 ( $500^\circ\text{C}$ ), ZnO-M2 ( $500^\circ\text{C}$ ), ZnO-M3 ( $750^\circ\text{C}$ ), and ZnO-M3 ( $900^\circ\text{C}$ ) are calculated from XRD line width to be 42.67 nm, 37.94 nm, 48.77 nm, and 37.42 nm, respectively. The lattice strain is 0.0027, 0.0031, 0.0024, and 0.0031, respectively, which indicates that ZnO-M3 ( $750^\circ\text{C}$ ) exhibits the lowest crystal imperfections. The lattice constant  $a=b$  are 3.2475 Å, 3.2377 Å, 3.2433 Å, and 3.2516 Å, respectively. However, the lattice constant  $c$  equals 5.2119 Å, 5.1901 Å, 5.1943 Å, and 5.209 Å, respectively and  $c/a$  ratio is 1.6049, 1.6030, 1.6015, and 1.6020, respectively. The positional parameter is 0.3794, 0.3797, 0.3799, and 0.3799, respectively. The Zn-O bond length is 1.9775 Å, 1.9708 Å, 1.9737 Å, and 1.9788 Å, respectively. Young's modulus is 118.8709 GPa, 118.8623 GPa, 118.8563 GPa,

and 118.8500 GPa. Morphology index is 0.5999, 0.5713, 0.6666 and 0.9312, respectively. The dislocation density is found to be  $5.49 \times 10^{-4} \text{ nm}^{-2}$ ,  $6.95 \times 10^{-4} \text{ nm}^{-2}$ ,  $4.20 \times 10^{-4} \text{ nm}^{-2}$ , and  $7.14 \times 10^{-4} \text{ nm}^{-2}$ , respectively, which is in accordance with

the lattice strain. ZnO-M3 (750°C) has the lowest lattice strain and therefore the minimum lattice dislocation. The Lorentz factor is 2.7139, 2.7017, 2.7116, and 2.7216. Lorentz polarization factor

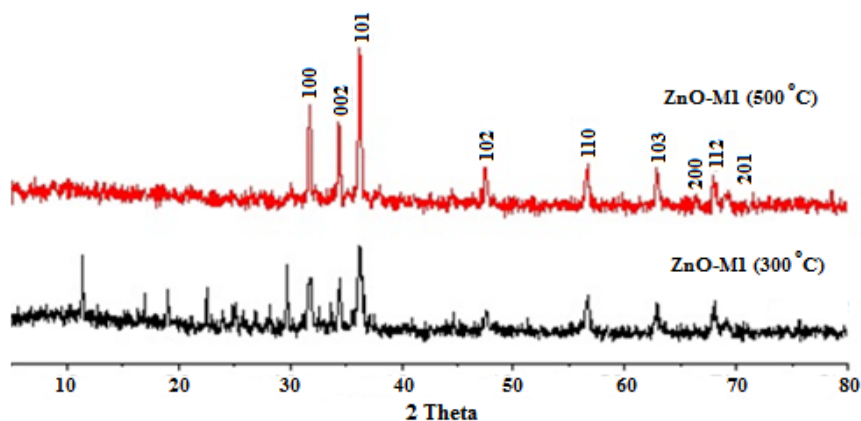


Fig. 2. XRD of ZnO-M1 (300°C) and ZnO-M1 (500°C).

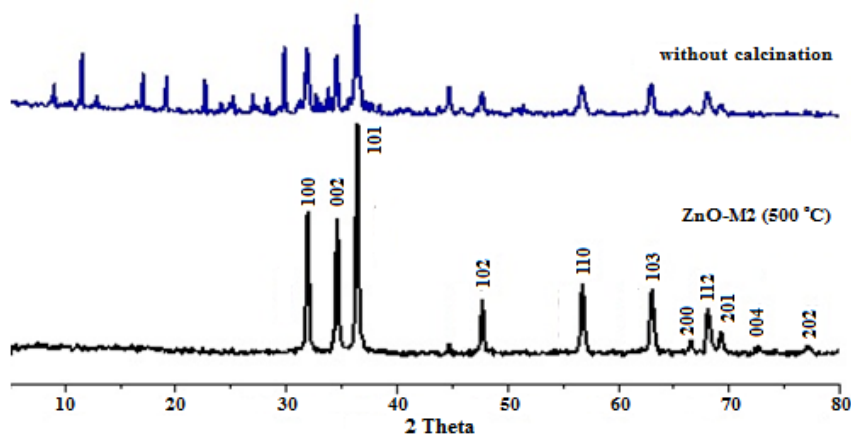


Fig. 3. XRD of ZnO-M2 (500°C) and ZnO NPs prepared by M2 without calcination.

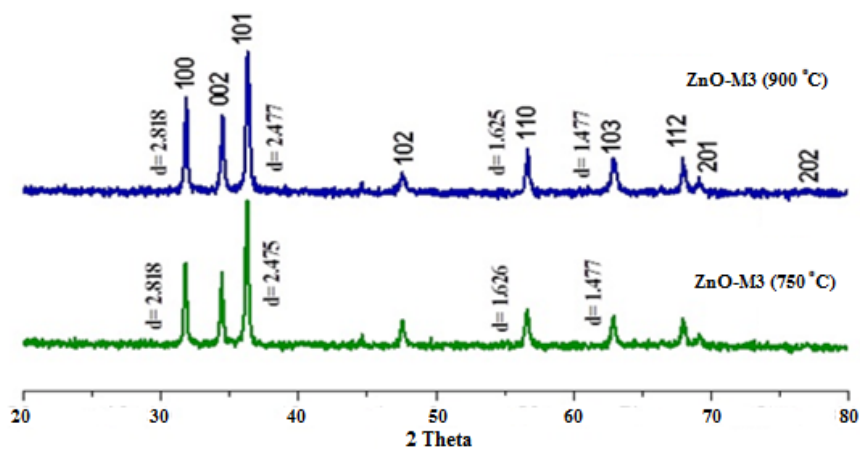


Fig. 4. XRD of ZnO-M3 (750°C) and ZnO-M3 (900°C).

is 17.9101, 17.8139, 17.8922, and 17.9715. The crystallite size (D) determined from Williamson-Hall plot of ZnO-M1 (500°C), ZnO-M2 (500°C), and ZnO-M3 (750°C) (**Fig. 5**) is 53.33 nm, 42.02 nm, and 45.67 nm, respectively. The isotropic microstrain determined from Williamson-Hall plot is 0.0017, 0.0002, and 0.0007, respectively. **Table 1** lists the XRD analysis of ZnO-M1 (500°C), ZnO-M2 (500°C), ZnO-M3 (750°C), and ZnO-M3 (900°C).

#### TEM and SEM images of the prepared ZnO NPs

TEM images of ZnO-M1 (500°C), ZnO-M2 (500°C), ZnO-M3 (750°C), and ZnO-M3 (900°C) are shown in **Fig. 6**. ZnO-M1 (500°C) prepared by sol-gel method shows a diversity of shapes; spherical, hexagonal, cubic, cuboid, unequal crystal faces and irregular particles. Therefore, a variety of diameters can be observed. The spherical particles are nearly all of the diameter close to 23-38 nm. However, the hexagonal crystals are ranged from 58 nm to 97 nm while some cuboid crystals exceed 100 nm. The rest of the particles have sizes that are ranged between the previous measurements. The ZnO NPs produced by the hydrothermal method are shown in ZnO-M2 (500°C) TEM image (**Fig. 6**). The predominant shapes are the spherical and irregular shapes with some hexagonal crystals. The particles are dominantly ranged between 30nm and 80nm. The TEM images of ZnO NPs prepared by the combustion method resulted in good crystallites. The TEM image of ZnO-M3 (750°C) shows complete clarity of hexagonal crystals that do not show this density in all other images. These crystallites represent a majority in the image with

dimensions ranged from 40 nm to more than 100 nm. Very little spherical particles can be detected with a size range below 40 nm. However, by increasing the calcination temperature up to 900°C using the combustion method, the majority of the particles tends to be spherical and irregular in shape. It is, therefore, possible to deduce through the TEM images that using the third method for the preparation of ZnO NPs (combustion method) and at calcination temperature 750°C can obtain the highest degree of hexagonal wurtzite crystals. The SEM micrographs of the prepared ZnO NPs are presented in **Fig. 7**. It can be illustrated from the images the difference in the morphological structure of ZnO-M3 (750°C) from the rest of the samples. A majority of spherical ZnO NPs are obtained by the three synthetic methods while different crystallites are obtained by the combustion method at calcination temperature 750°C.

ZnO-M3 (750°C) was selected amongst the other prepared ZnO NPs to be modified with PANI and produce the PANI/ZnO NCs. This selection was based on the better crystallographic hexagonal wurtzite structure of ZnO NPs synthesized by M3 at 750°C than those produced with the other methods. In addition, ZnO-M3 (750°C) exhibited the lowest crystal imperfections.

#### FTIR of PANI/ZnO NCs

The FTIR spectra of NC10, NC15, and NC20 are given in **Fig. 8**. The band characteristic to Zn-O stretching obviously appeared at 480 cm<sup>-1</sup> associated with a shoulder at 500 cm<sup>-1</sup> which is similar to that occurred in **Fig. 1**. The other bands attributed to ZnO NPs appeared at 1625cm<sup>-1</sup> and

**TABLE 1.** XRD analysis of ZnO-M1 (500°C), ZnO-M2 (500°C), ZnO-M3 (750°C), and ZnO-M3 (900°C).

Parameter	ZnO NPs			
	ZnO-M1 (500°C)	ZnO-M2 (500°C)	ZnO-M3 (750°C)	ZnO-M3 (900°C)
D	42.67	37.94	48.77	37.42
Lattice strain	0.0027	0.0031	0.0024	0.0031
Lattice constants a = b (Å°)	3.2475	3.2377	3.2433	3.2516
Lattice constants c (Å°)	5.2119	5.1901	5.1943	5.2091
c/a ratio	1.6049	1.6030	1.6015	1.6020
Positional parameter	0.3794	0.3797	0.3799	0.3799
Zn-O bond length	1.9775	1.9708	1.9737	1.9788
Lorentz factor	2.7139	2.7017	2.7116	2.7216
Lorentz polarization factor	17.9101	17.8139	17.8922	17.9715
Dislocation density (nm <sup>-2</sup> )	5.49×10 <sup>-4</sup>	6.95×10 <sup>-4</sup>	4.20×10 <sup>-4</sup>	7.14×10 <sup>-4</sup>
Morphology index.	0.5999	0.5713	0.6666	0.9312
Young's modulus GPa	118.8709	118.8623	118.8563	118.8500

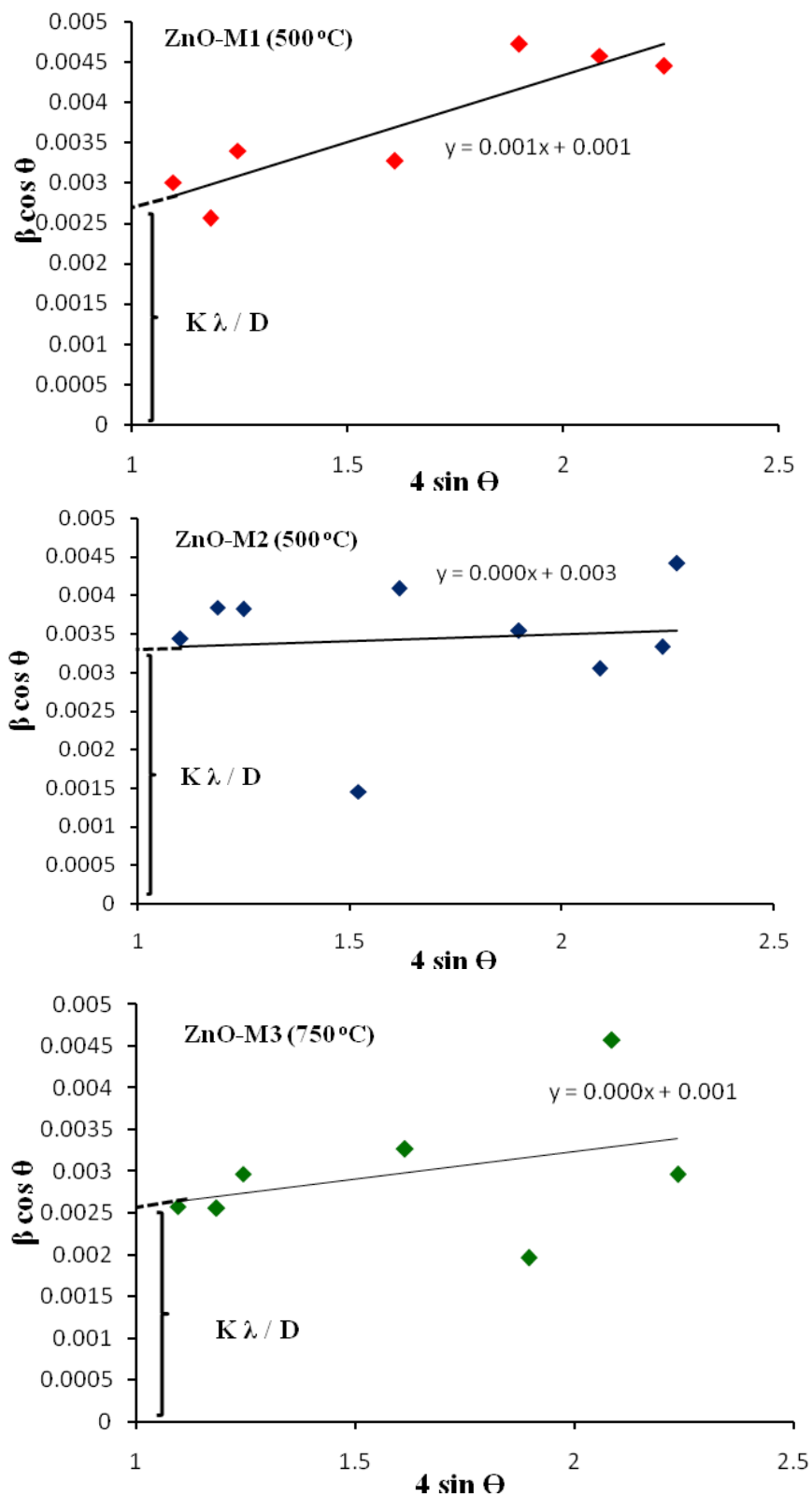
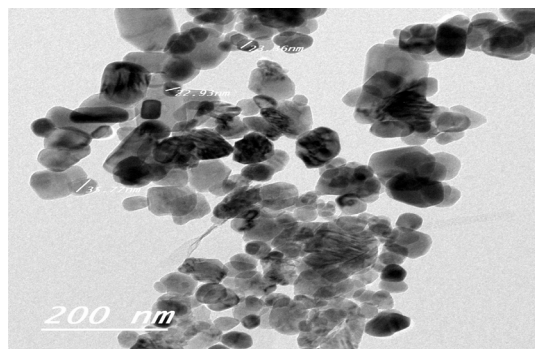
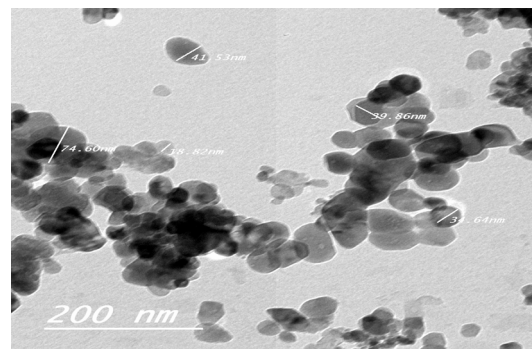


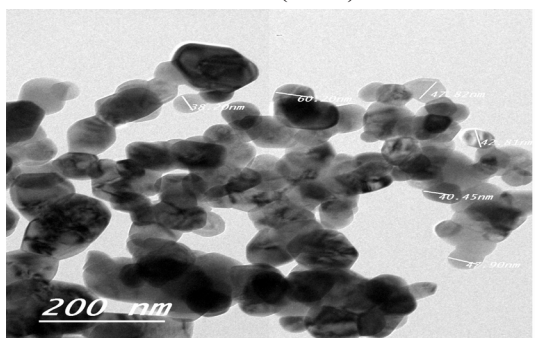
Fig. 5. Williamson-Hall plots of ZnO-M1 (500 °C), ZnO-M2 (500 °C), and ZnO-M3 (750 °C).



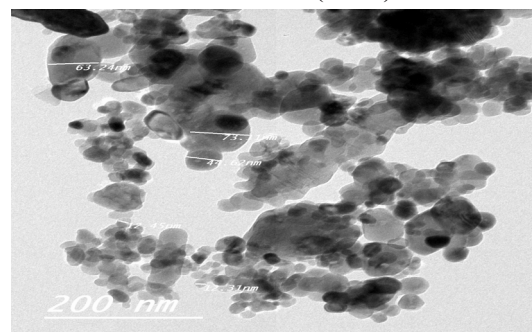
ZnO-M1 (500°C)



ZnO-M2 (500°C)

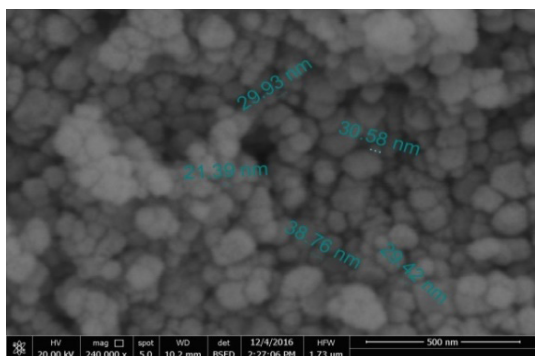


ZnO-M3 (750°C)

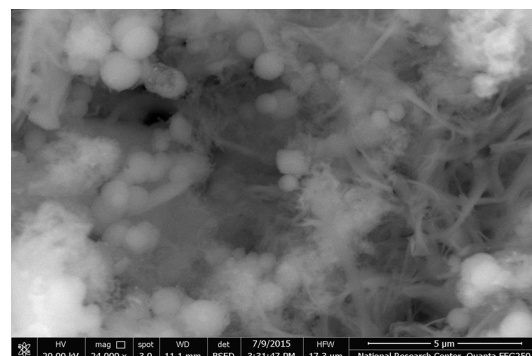


ZnO-M3 (900°C)

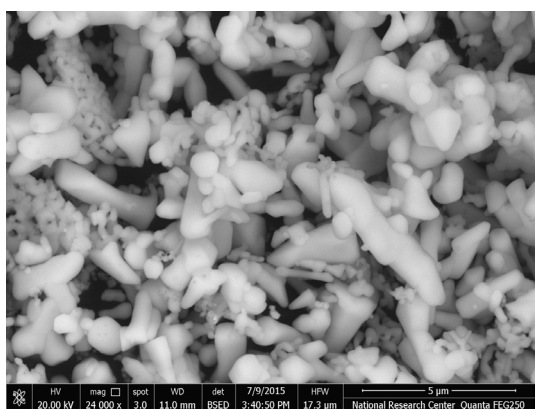
Fig.6. TEM images of ZnO-M1 (500°C), ZnO-M2 (500°C), ZnO-M3 (750°C), and ZnO-M3 (900°C).



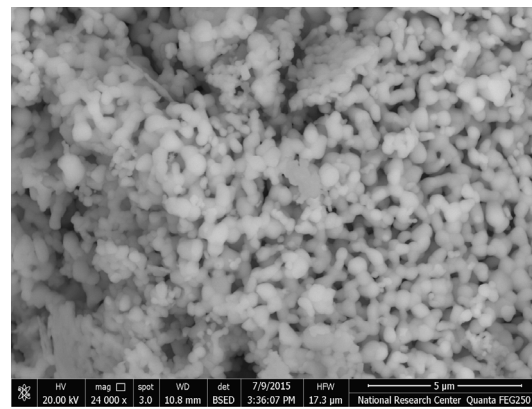
ZnO-M1 (500°C)



ZnO-M2 (500°C)



ZnO-M3 (750°C)



ZnO-M3 (900°C)

Fig. 7. SEM images of ZnO-M1 (500°C), ZnO-M2 (500°C), ZnO-M3 (750°C), and ZnO-M3 (900°C).

3497  $\text{cm}^{-1}$  attributed to  $\text{H}_2\text{O}$  and O-H stretchings. However, the distinctive bands of PANI emerged in all the spectra of the PANI/ZnO NCs. The bands at 1569  $\text{cm}^{-1}$  and 1500  $\text{cm}^{-1}$  are attributed to stretching of quinonoid and benzenoid rings in PANI, respectively [30]. The absorption peak located at 1384  $\text{cm}^{-1}$  corresponds to C-N stretching. The bands at 1040 and 866  $\text{cm}^{-1}$  are due to in-plane and out of plane bending vibrations,

respectively.

#### XRD of PANI/ZnO NCs

XRD patterns of PANI/ZnO NCs are presented in Fig. 9. The characteristic peaks of ZnO NPs are clearly detected in the three XRD graphs of NC10, NC15, and NC20. The lattice planes of ZnO NPs are observed including (100), (002), (101), (102), (110), (103), (200), (112), (201), and (004) planes. A new peak emerges at  $2\theta \sim 6.2^\circ$

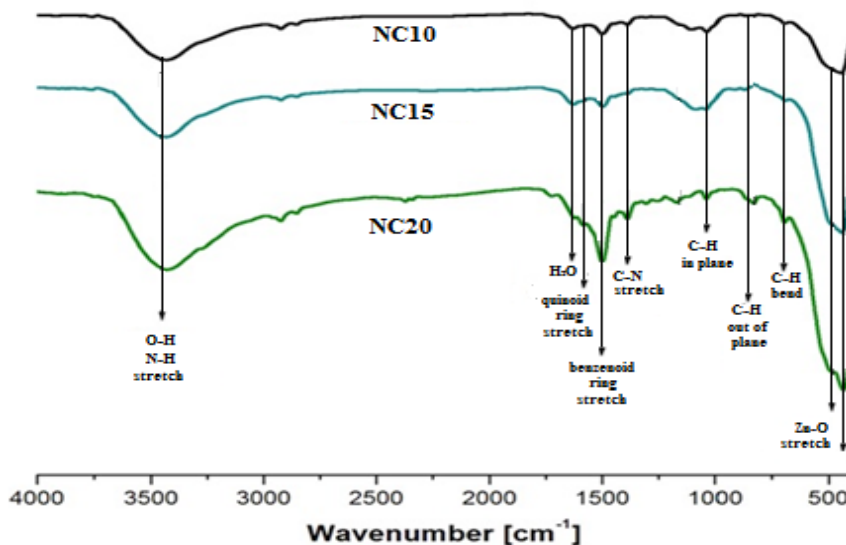


Fig. 8. FTIR of PANI/ZnO NCs.

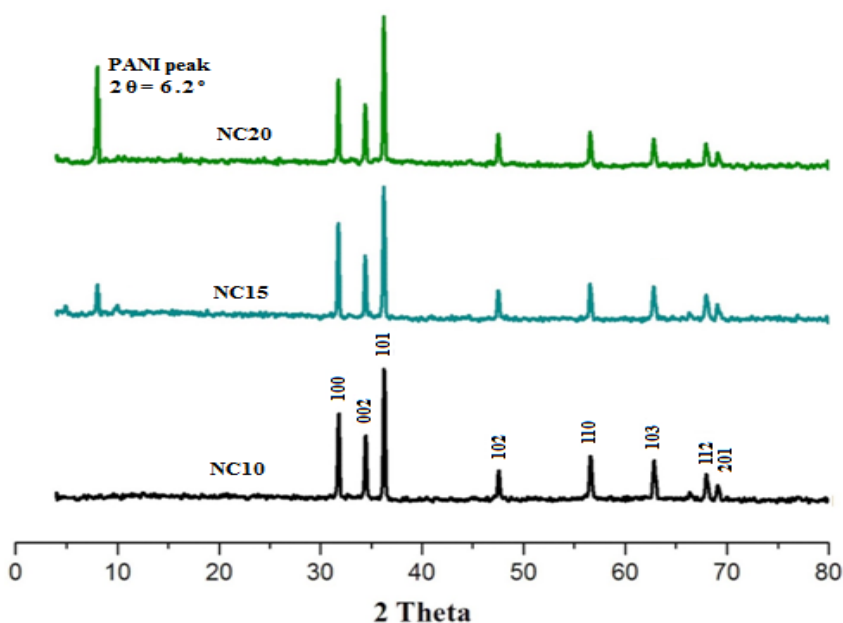


Fig. 9. XRD of PANI/ZnO NCs.

in XRD of NC15 and NC20. However, this peak does not exist at low PANI concentration (XRD of NC10). This peak is related to the periodicity along the PANI chains which arise at high PANI concentration in the NCs.

#### TEM and SEM images of PANI/ZnO NCs

The TEM image of NC20 is shown in **Fig. 10**. Some PANI appeared as a fibrous-rod like structures. This shape is formed through the chain reaction between the aniline monomers that are connected in a head-to-tail mode during the polymerization process. Other PANI appeared in an amorphous shape that predominates in the matrix and covers the ZnO NPs. The SEM micrographs of PANI and NC20 are presented in **Fig. 11**. The morphology of PANI (**Fig. 11a**) appears in sponges, representing the amorphous phase, and fibers. These fibers and sponges exist

in the NC20 image (**Fig. 11b**) beside the granular ZnO NPs.

#### Antimicrobial activity of PANI/ZnO NCs

The antimicrobial activity of the synthesized PANI/ZnO NCs against bacteria and fungi was evaluated relative to standards. The results are listed in **Table 2** and the zone inhibition around the film samples are shown in **Fig. 12**. For the antibacterial test, the results revealed that all PANI/ZnO NCs have medium antibacterial activity against *Escherichia coli* (G<sup>-</sup>) and *staphylococcus aureus* (G<sup>+</sup>) except for NC15 which exhibits high efficiency against *staphylococcus aureus* (G<sup>+</sup>). However, for the antifungal activity, there was no efficiency of all PANI/ZnO NCs against *Aspergillus flavus* while medium activity was observed by all PANI/ZnO NCs against *Candida albicans* except for NC15 that again showed a

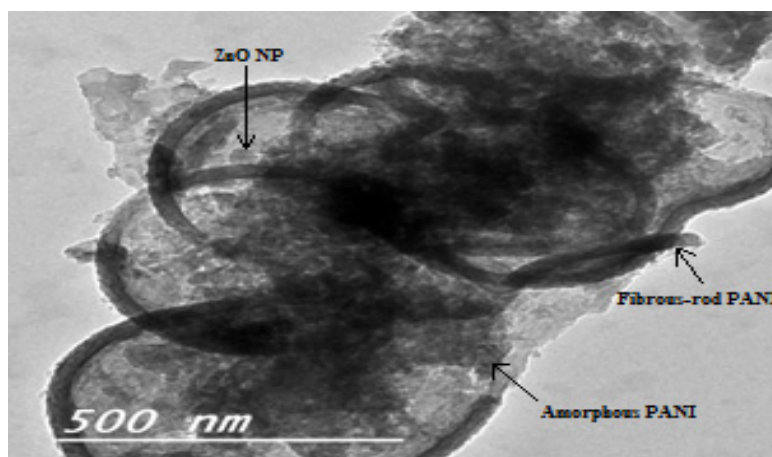
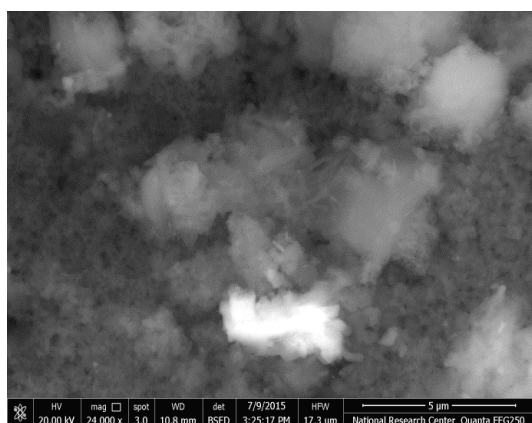
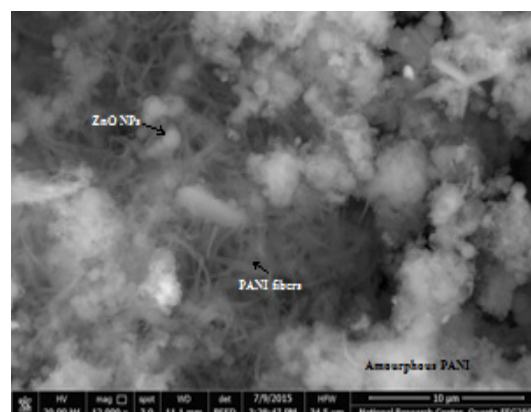


**Fig. 10.** TEM image of NC20.



**(a)**



**(b)**

**Fig. 11.** SEM micrographs of PANI (a) and NC20 (b).

high efficiency.

Generally, the antimicrobial activity of PANI/ZnO NCs is mainly attributed to the effect of ZnO NPs. The photocatalytic efficiency of the ZnO NPs enables them to generate reactive oxygen

species (such as  $H_2O_2$ ) on the surface of the particles. These species penetrate the cell wall and kill the microbe. The increased antimicrobial activity of NC15 than NC10 may be explained by the role of PANI in PANI/ZnO NCs in enhancing

TABLE 2. Antimicrobial activity of PANI/ZnO NCs.

Sample	Inhibition zone diameter ( mm/mg sample )							
	<i>Escherichia coli</i> (G <sup>-</sup> )		<i>Staphylococcus aureus</i> (G <sup>+</sup> )		<i>Aspergillus flavus</i>		<i>Candida albicans</i>	
Control : DMSO	0.0		0.0		0.0		0.0	
Ampicillin antibacterial agent	25		21		--		--	
Amphotericin B Antifungal agent	--		--		16		19	
Standard	% to Standard		% to Standard		% to Standard		% to Standard	
	NC10	14	12.14	57.80	0	11	57.89	
	NC15	14	14.66	69.81	0	13	68.42	
	NC20	12	12.00	57.14	0	10	52.63	

Values with respect to standards: 30%, 30-60%, and > 60% are considered weak, medium and high, respectively.

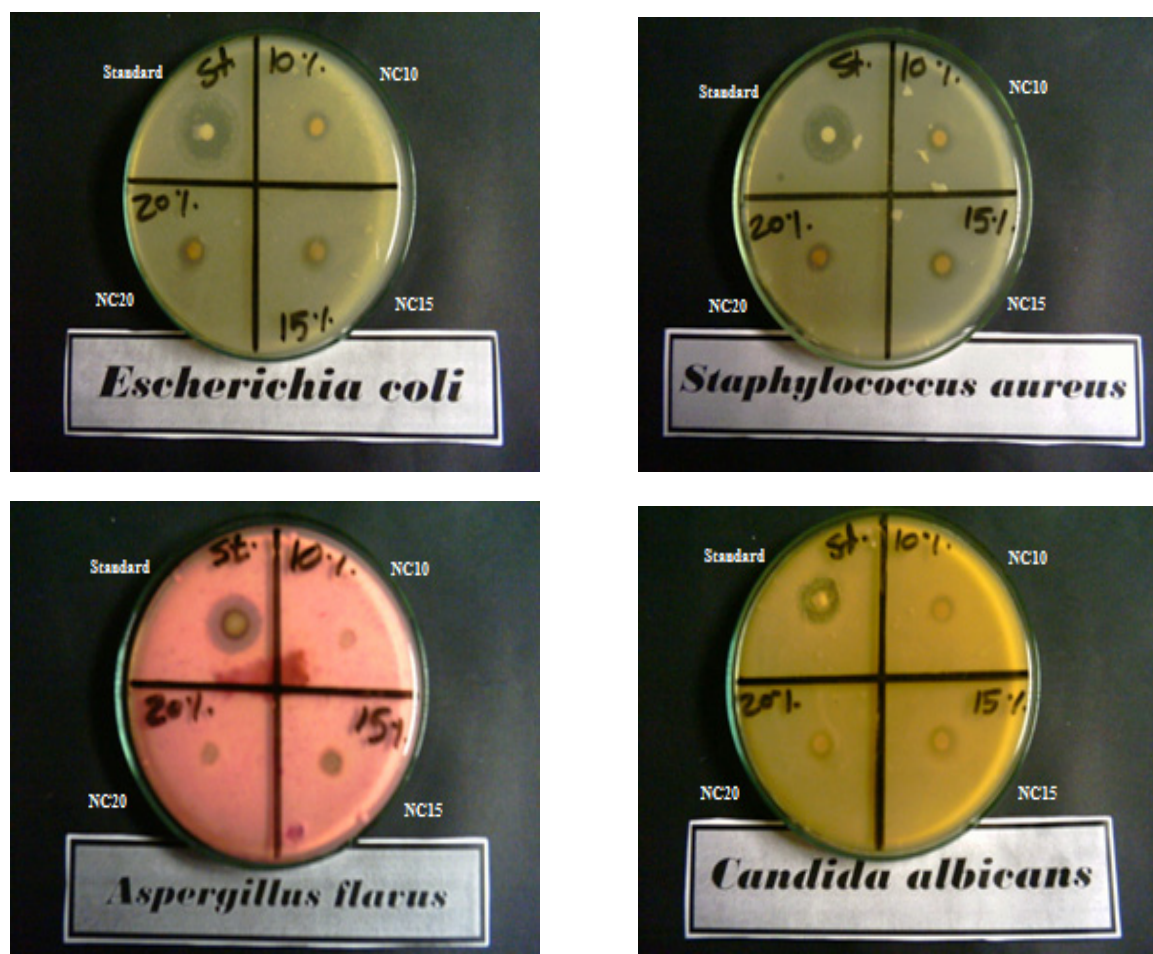


Fig. 12. Antimicrobial activity images of PANI/ZnO NCs by agar well diffusion method.

the photocatalytic activity of ZnO NPs. The high mobility of photo-induced holes in PANI promotes the separation efficiency of electron-hole pairs in the ZnO NPs [5,31]. However, the subsequent decrease in the antimicrobial activity in NC20 may be attributed to the high content of PANI in NC20 relative to the other NCs. PANI covers the effective toxicant ZnO NPs which have the real effect in killing the microbes. The noticeable higher antibacterial efficiency of the NCs than their antifungal activity can be due to the electrostatic interaction that is generated between the positively charged surface of doped PANI and the negative bacterial surface. However, the very slight higher efficiency of the NCs against *Staphylococcus aureus* ( $G^+$ ) than *Escherichia coli* ( $G^-$ ) is due to the easier penetration of the ionized PANI into the hydrophilic  $G^+$  membrane than the hydrophobic lipid bilayers  $G^-$  membrane.

### Conclusion

ZnO NPs had been prepared using three different methods; sol-gel, hydrothermal, and combustion methods followed by characterization using FTIR, XRD, TEM, and SEM. The analysis confirmed that the calcination temperature has a great effect on the purity, morphological, and crystallographic properties of the produced ZnO NPs. The results proved that the temperature of calcination should be higher than 300°C to obtain pure and clear ZnO NPs. The FTIR spectra of the prepared NPs confirmed the formation of ZnO by the emergence of two transverse optical stretching modes of Zn-O at 472  $\text{cm}^{-1}$  and 500  $\text{cm}^{-1}$ . The XRD analysis pointed out that the size of the produced ZnO NPs was ranged between 48.77-37.42 nm while their shape was detected from TEM images. The majority of ZnO-M1 (500°C), ZnO-M2 (500°C), and ZnO-M3 (900°C) particles were spherical while a polycrystalline wurtzite hexagonal structure was the predominant in ZnO-M3 (750°C) image. The strain-induced broadening, the lattice constant, isotropic microstrain, bond length, morphology index, Young's modulus, dislocation density, and Lorentz polarization factor of the prepared ZnO NPs were estimated. ZnO-M3 (750°C) exhibited the lowest crystal imperfections and was selected to prepare three different NCs with PANI (NC10, NC15, and NC15) by *in-situ* polymerization of aniline on the dispersion of its NPs. The NCs were characterized by XRD, FTIR, TEM, SEM, and antimicrobial activity. The characteristic absorption peaks of PANI emerged in the FTIR of

PANI/ZnO NCs. TEM image showed that PANI appeared in the form of amorphous shape and fibrous-rod structures covering the ZnO NPs in the NCs. The enhancement of the photocatalytic activity of ZnO NPs was detected by the higher antimicrobial efficiency of NC15 than NC10. However, the increased amounts of PANI (NC20) resulted in a subsequent decrease in the antimicrobial activity due to the covering of the effective agent ZnO NPs. The NCs exhibited higher toxicity against bacteria than fungi. This is due to the generation of electrostatic interaction between the positively charged surface of doped PANI and the negative bacterial surface. The NCs showed higher antibacterial efficiency against *Staphylococcus aureus* ( $G^+$ ) than *Escherichia coli* ( $G^-$ ). The hypothesis is that the NCs penetrated into the hydrophilic *Staphylococcus aureus* ( $G^+$ ) membrane easier than the hydrophobic lipid bilayers  $G^-$  membrane. This is because of the ionized PANI and the hydroxyl groups loaded on the surface of the ZnO NPs.

### Acknowledgement

Great appreciation to National Research Center for the financial support of this research article derived from project No.10050408 (2013-2016). Deep thanks to Prof. Dr. Mohamed Hashem President of National Research Center for his continuous support.

### References

1. Mohsen. R.M., Selim, M.M., Abu-Ayana, Y.M., Morsi, S.M.M., Ghoneim, A.M., El-Sawy S.M., *Nanotechnology and Nanomaterials*, Chap. 7 in *Nanomaterials & Nanotechnology*, One Central Press (OCP). 145-179 (2016).
2. Radzimska, A.K., Jesionowski, T., Zinc Oxide—from synthesis to application: A Review, *Mater.*, **7**, 2833-2881 (2014).
3. Matei, A., Tucureanu, V., Dumitrescu, L., Aspects regarding synthesis and applications of ZnO nanomaterials. *Bulletin of the Transilvania Univ. of Brasov*, **7**, 45-52 (2014).
4. Kumra, K.M., Mandal, B.K., Naidu, E.A. Sinha, M., Kumar, K.S., Reddy, P.S., Synthesis and characterization of flower shaped zinc oxide nanostructures and its antimicrobial activity. *Spectrochim. Acta Part A Mol. Biomol. Spectrosc.*, **104**, 171–174 (2013).

5. Mohsen, R.M., Morsi, S.M.M., Selim, S.M.M., Ghoneim, A.M., El-Sherif, H.M., Electrical, thermal, morphological, and antibacterial studies of synthesized polyaniline/zinc oxide nanocomposites. *Polym. Bull.*, (in press).
6. Hassan, F., Miran, M.S., Simol, H.A., Susan, M.A.B., Mollah, M.Y.A., Synthesis of ZnO nanoparticles by a hybrid electrochemical-thermal method: influence of calcination temperature. *Bangladesh J. Sci. Ind. Res.*, **50**, 21-28 (2015).
7. Raj, K.P., Sadayandi, K., Effect of temperature on structural, optical and photoluminescence studies on ZnO nanoparticles synthesized by the standard co-precipitation method. *Physica B: Condensed Matter*, **487**, 1-7 (2016).
8. Zak, A.K., Abrishami, E., Abd. Majid, W.H., Yousefi R., Hosseini, S.M., Effects of annealing temperature on some structural and optical properties of ZnO nanoparticles prepared by a modified sol-gel combustion method. *Ceram. Int.*, **37**, 393-398 (2011).
9. Parra, M.R., Haque, F.Z., Aqueous chemical route synthesis and the effect of calcination temperature on the structural and optical properties of ZnO nanoparticles. *J. Mater. Res. Technol.*, **3**, 363-369 (2014).
10. Stanković, A., Veselinović, L.J., Skapin, S.D., Marković, S., Uskoković, D., Controlled mechanochemically assisted synthesis of ZnO nanopowders in the presence of oxalic acid, *J. Mater. Sci.*, **46**, 3716–3724 (2011).
11. Lanje, A.S., Sharma, S.J., Ningthoujam, R.S., Ahn, J.S., Pode, R.B., Low temperature dielectric studies of zinc oxide (ZnO) nanoparticles prepared by precipitation method. *Adv. Powder Technol.*, **24**, 331–335 (2013).
12. Ramadan, M.A., Nassar, S.H., Montaser, A.S., El-Khatib E.M., Abdel-Aziz M.S., Synthesis of nano-sized zinc Oxide and its application for cellulosic textiles. *Egyptian J. Chem.*, **59**, 523-525 (2016).
13. Morshedy, A.S., El Nagger, A.M.A., Tawfik, S.M., El-Din, O.I.S., Hassan S.I., Hashem, A.I., Preparation and characterization of micro-porous ZnO nanoparticles. *Egyptian J. Chem.*, **59**, 609–621 (2016).
14. Jesionowski, T., Radzimska, A.K., Ciesielczyk, F., Ledakowicz, J.S., Olczyk, J., Sielski, J., Synthesis of Zinc Oxide in an Emulsion System and its Deposition on PES Nonwoven Fabrics. *Fibers Text. East. Eur.*, **19**, 70-75 (2014).
15. Bari, A.R., Shinde, M.D., Deo, V., Patil, L.A., Effect of solvents on the particle morphology of nanostructured ZnO. *Indian J. Pure Appl. Phys.*, **47**, 24-27 (2009).
16. Ristic, M., Music, S., Ivanda, M., Popovic, S., Sol-gel synthesis and characterization of nanocrystalline ZnO powders. *J. Alloys Compod.*, **39**, L1- L4 (2005).
17. Schneider, J.J., Hoffmann, R.C., Engstler, J., Klyszcz, A., Erdem, E., Jakes, P., Eichel, R.A., Bauermann, L.P., Bill, J., Synthesis, characterization, defect chemistry, and FET properties of microwave-derived nanoscaled zinc oxide. *Chem. Mater.*, **22**, 2203–2212 (2010).
18. Ismail, A.A., El-Midany, A., Abdel-Aal, E.A., El-Shall, H., Application of statistical design to optimize the preparation of ZnO nanoparticles via hydrothermal technique. *Mater. Lett.*, **59**, 1924–1928 (2005).
19. Noori, N.R., Mamoory, R.S., Alizadeh, P., Mehdikhani, A., Synthesis of ZnO nano powder by a gel combustion method. *J. Ceram. Process. Res.*, **9**, 246-249 (2008).
20. Banerjee, P., Chakrabarti, S., Maitra S., Dutta B.K., Zinc oxide nano-particles-sonochemical synthesis, characterization and application for photo-remediation of heavy metal. *Ultrason. Sonochem.*, **19**, 85-93 (2012).
21. Sharma, S., Singh, S., Khare, N., Enhanced photosensitization of zinc oxide nanorods using polyaniline for efficient photocatalytic and photoelectrochemical water splitting, *Int. J. Hydrog. Energy*, **41**, 21088-21098 (2016).
22. Espitia, P.J.P., Soares, N.F.F., Coimbra, J.S.R., Andrade, N.J., Cruz, R.S., Medeiros, E.A.A., Zinc Oxide nanoparticles: Synthesis, antimicrobial activity and food packaging applications, *Food Bioprocess Technol.*, **5**, 1447–1464 (2012).
23. Kermani, A.S., Mirzaee, M., Moghaddam, M.G., Polyvinyl alcohol/Polyaniline/ZnO nanocomposite:

- Synthesis, Characterization and Bactericidal Property. *Adv. Biol. Chem.*, **6**, 1-11 (2016).
24. Khan, J.S., Radhakrishnan, A., Beena, B., Polyaniline/Zinc Oxide Nanocomposite as a Remarkable Antimicrobial Agent in Contrast with PANI and ZnO. *Indian J. Adv. Chem. Sci.*, **6**, 71-76 (2018).
25. Hou, Y., Feng, J., Wang, Y., Li, L., Enhanced antibacterial activity of Ag-doped ZnO/polyaniline nanocomposites, *J. Mater. Sci. Mater. Electron.*, **27**, 6615–6622 (2016).
26. Mohsen, R.M., Morsi, S.M.M., Abu-ayana, Y.M., Ghoneim, A.M., Synthesis of conductive Cu-core / Ag-subshell / polyaniline-shell nanocomposites and their antimicrobial activity. *Egyptian J. Chem.*, **61**, 590-600 (2018).
27. Parra, M.R., Haque, F.Z., Aqueous chemical route synthesis and the effect of calcination temperature on the structural and optical properties of ZnO nanoparticles. *J. of Materials Research and Technology*, **3**, 363-369 (2014).
28. Bauer, A.W., Kirby, W.M., Sherris, J.C., Turck, M., Antibiotic susceptibility testing by a standardized single disk method, *Am. J. Clin. Pathol.*, **45**, 493-496 (1966).
29. Kuthirummal, N., Smith, G.M., Lopez, L., Podila, R., Howell, J., Dun, C., Rao A.M., Synthesis and characterization of Ar-annealed zinc oxide nanostructures, *AIP Adv.*, **6**, 095225 (2016).
30. Morsi, S.M.M., Emira, H.S., El-Sawy, S.M., Mohsen, R.M., Khorshed, L.A., Synthesis and characterization of kaolinite/polyaniline nanocomposites and investigating their anticorrosive performance in chlorinated rubber/alkyd coatings. *Polym. Compos.*, in press.
31. Liang, X., Sun, M., Li, L., Qiao, R., Chen, K., Xiao Q., Xu, F., Preparation and antibacterial activities of polyaniline/Cu<sub>0.05</sub>Zn<sub>0.95</sub>O nanocomposites. *Dalton Trans.*, **41**, 2804–2811 (2012).

### تحضير جسيمات أكسيد الزنك النانومترية الحجم بواسطة تقنيات الصول جل، الهيدروحرارية، الاحتراق المحورة بالبولى أنيلين للتطبيق كمتراكبات مضادة للميكروبات

سمير مرسى محمد<sup>١</sup>، راجيه محسن<sup>١</sup>، محمد محمد سليم<sup>١</sup> و حازم الشريف<sup>٢</sup>

<sup>١</sup>شعبة الصناعات الكيماوية - قسم البوليمرات والمخضبات - المركز القومى للبحوث - الجيزة - مصر.

<sup>٢</sup>شعبة الصناعات الغير عضويه والتعدين - قسم الكيمياء الفيزيائية - المركز القومى للبحوث - الجيزة - مصر.

يهدف هذا البحث لتحضير أكسيد الزنك المحضر النانومترى الحجم لأستخداماته المتعددة فى شتى المجالات التطبيقية. وقد تم التحضير بثلاث طرق كيميائية (الصول جل و الهيدرو حراري والاحتراق) وتم دراسة استخدام درجات معالجة حرارية مختلفه لدراسة تأثيرها على الخواص المميزة لبودرة أكسيد الزنك المحضر من حيث حجم وشكل الجسيمات النانومترية المحضرة. وقد تم التوصيف باستخدام الأشعة السينيه و طيف الأشعة تحت الحمراء وايضا باستخدام الميكروسكوب الماسح الألكترونى وايضا الميكروسكوب ذو النفاذيه. وقد تم أستنتاج أن درجة المعالجه الحراريه ذات تأثير على شكل وحجم الجسيمات النانومترية لأكسيد الزنك المحضر . وقد اثبتت القياسات بالأشعة تحت الحمراء ان ماده المحضرة هي أكسيد الزنك . كما ان الأشعة السينيه أثبتت نقاوة أكسيد الزنك المحضر وأنه ذو شكل بلورات سداسيه نانومترية الحجم تختلف طبقا للطريقة المستخدمة. وطبقا للميكروسكوب ذو النفاذيه فالجسيمات النانومترية ذو شكل مكعبى اما الميكروسكوب الماسح فقد بين أن جسيمات اكسيد الزنك المحضر كرويه الشكل وقد تحتوى على قضبان حسب طريقة التحضير . كما تم تحضير متراكب بوليمرى نانومترى الحجم من البولى أنيلين - اكسيد الزنك النانومتري بثلاث نسب من البولى أنيلين ( ١٠% ، ١٥% ، ٢٠% ) وتم التوصيف بكل من الأشعة السينيه التى أعطت نفس الشكل مثل أكسيد الزنك النانومتري والأشعة تحت الحمراء والتي اكدت التركيب الكيماوى للبولى أنيلين والقوة الرابطة مع أكسيد الزنك النانومتري . وتم التصوير بالميكروسكوب الالكترونى الذى أوضح ان اكسيد الزنك قد أحاط بشكل حلقات حول البولى أنيلين . أما الميكروسوب الألكترونى الماسح أوضح ان سطح المتراكب على شكل اسفنجى . كما تم تقييم مقاومة المتراكبات المحضرة للميكروبات (نوعين من البكتريا ونوعين من الفطريات) واثبتت كفاءتها الجيدة.